Pressure Distribution under Steel and Timber Crossties in Railway Tracks

Weimin Song[1]; Xiang Shu, Ph.D., A.M.ASCE[2]; Baoshan Huang, Ph.D., P.E., M.ASCE[3]; Yiren Sun[4]; Hongren Gong[5]; and David Clarke, Ph.D.[6]

Abstract: The pressure distribution under the crossties plays a key role in railroad performance. This study conducts laboratory testing to investigate the pressure distributions under two different types of crossties, steel and timber. For each type, this study employs only a single tie. Five pressure cells are placed equidistantly under the rail crosstie between the two rails to measure the pressure distribution. Both static and cyclic loadings are applied during the test. The pressure distributions are compared between the steel and timber crossties. The effect of the cyclic loading on the pressure distribution also is explored. It is found that pressure distribution is different for steel and timber crossties. Cyclic loading could change the pressure distribution under both steel and timber crossties, but the effect of cyclic loading is more obvious on the steel crosstie than on the timber crosstie. Differences exist in pressure distribution between loading and unloading processes. **DOI: 10.1061/JTEPBS.0000075.**

Author keywords: Pressure distribution; Railroad track; Timber crosstie; Steel crosstie; Cyclic loading.

Introduction

The rapid development of railroad transportation requires a longer service life of the crossties and safer train travel. Research on the pressure distribution under crossties offers a better understanding of the interactions between ballast and crossties, and further provides assistance for rail transportation guidelines.

Two main types of railroad track are used in the world: track supported by ballast, and ballastless track. The ballastless track is designed mainly for high-speed railway transit. For the ballasted track system, crossties and ballast are two key components. Timber crossties account for approximately 90–95% of all the crossties in the United States (Csenge et al. 2015). Steel crossties make up only a very small part and generally are used for light-density secondary track. Although timber ties are more widely used in the United States, light rail transit systems constructed with timber ties need to replace a large percentage of the timber crossties after a service life of only 20–30 years (Brinckerhoff 2012). In contrast, steel crosstie usage is steadily rising because of such benefits as a long service life, easy installation, and cost effectiveness. In addition to timber and steel crossties, concrete crossties are also used in the United States.

Pressure distribution under crossties is of great importance to a railway track system. Previous research has shown that the tie-to-ballast pressure is not uniformly distributed under the ties. The American Railway Engineering and Maintenance-of-Way Association (AREMA) recommends that the calculation of the pressure should take into account the distribution and impact factors (AREMA 2016). In railway track design, AREMA proposes four equations describing the relationships between the tie-to-ballast pressure and other parameters, including ballast depth and wheel load (AREMA 2016). McHenry et al. (2015) conducted one field test to determine the stress distribution under timber and concrete crossties and considered such factors as the contact area between the ballast and crossties. Laryea et al. (2014) compared the stress distribution under concrete crossties and steel crossties. They found that for the concrete crossties, the load mainly is transferred vertically. However, the steel crosstie section presents a large force concentration under its edge while a significant part of the load is still vertically transmitted through the underside of the crosstie. After one million cycles of loading, the stress at the center of the steel crosstie is higher than that beneath the rail seats. However, for the concrete crosstie, the stress beneath the rail seat is larger after cyclic loading, and the pressure distribution follows a parabolic pattern (Laryea et al. 2014; Sadeghi 2008, 2010).

The testing setup of the pressure distribution measurement plays an important role in the accuracy of the results. In some studies, pressure cells were placed at the interface between ballast and crossties (McHenry et al. 2015; Sadeghi 2008, 2010). In other studies, pressure cells were placed on ballast and the crossties were placed on the pressure cells. This setup method may cause inadequate contact between crosstie and ballast, especially when the pressure cells are thick. Some researchers embedded pressure cells within the bottoms of the ties so that the surfaces of the pressure plates would be flush with the bottoms of the ties (Sadeghi 2008, 2010). This method could give more reliable test results.

In addition to laboratory tests and filed tests, the discrete-element method and the finite-element method have been used

[1]Graduate Research Assistant, Dept. of Civil and Environmental Engineering, Univ. of Tennessee, Knoxville, TN 37996. E-mail: wsong8@vols.utk.edu

[2]Research Assistant Professor, Dept. of Civil and Environmental Engineering, Univ. of Tennessee, Knoxville, TN 37996. E-mail: xshu@utk.edu

[3]Professor, Dept. of Civil and Environmental Engineering, Univ. of Tennessee, Knoxville, TN 37996 (corresponding author). ORCID: https://orcid.org/0000-0001-8551-0082. E-mail: bhuang@utk.edu

[4]Graduate Research Assistant, School of Transportation and Logistics, Dalian Univ. of Technology, Dalian 116024, China. E-mail: ysun47@utk.edu

[5]Graduate Research Assistant, Dept. of Civil and Environmental Engineering, Univ. of Tennessee, Knoxville, TN 37996. E-mail: hgong2@vols.utk.edu

[6]Research Associate Professor, Center of Transportation Research, Univ. of Tennessee, Knoxville, TN 37996. E-mail: dclarke@utk.edu

Note. This manuscript was submitted on December 7, 2016; approved on April 10, 2017; published online on July 7, 2017. Discussion period open until December 7, 2017; separate discussions must be submitted for individual papers. This paper is part of the ***Journal of Transportation Engineering, Part A: Systems***, © ASCE, ISSN 2473-2907.

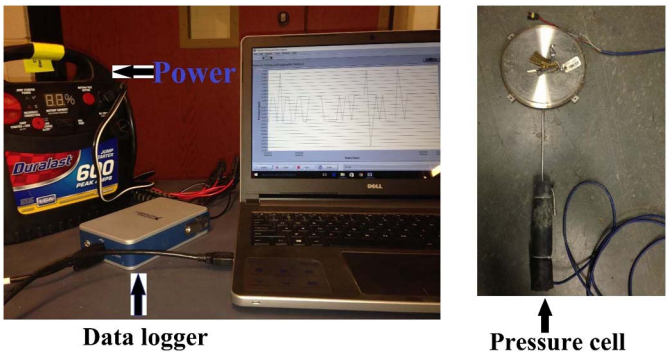

Fig. 1. System for pressure distribution measurement components (images by Weimin Song)

in the research of ballast under static and cyclic loadings (Hossain et al. 2007; Indraratna et al. 2009; Kuo and Huang 2009; Recuero et al. 2011). Ballast degradations are observed under the external load and especially under cyclic loading, so the crossties cannot be fully supported by the ballast, which may accelerate the degradation of the crossties (Anderson and Fair 2008; Hossain et al. 2007; Indraratna et al. 2009; Recuero et al. 2011; Sun et al. 2015).

In the research of crosstie behavior or the pressure distribution under crossties, many techniques have been employed, including matrix-based tactile surface sensors (McHenry et al. 2015; Rapp et al. 2013; Rose et al. 2004), Geokon pressure cells (Anderson and Rose 2008; Jia et al. 2009; Rose et al. 2004), and strain gauges (Wolf et al. 2015). This study used Geokon (Lebanon, New Hampshire) pressure cells to measure the pressure distribution.

This study investigated the pressure distribution under steel and timber crossties through laboratory testing. The pressure distributions under steel and timber crossties were compared and analyzed. The effect of cyclic loading on the pressure distribution under the ties also was examined.

System for Pressure Distribution Measurement

This system was composed of four components: (1) a power source which provides excitation voltage; (2) a data acquisition device; (3) pressure cells; and (4) a computer running the data acquisition and analysis software (Fig. 1).

A pressure cell is fabricated by welding together two steel plates, leaving a narrow space between them filled with hydraulic oil. The hydraulic oil is connected hydraulically to a pressure transducer, in which the oil pressure is converted into an electrical signal which can be read by the computer. This study used pressure cells with a surface area of 0.03 m^2. The data acquisition device (NI 9203) had 10 terminals. The data logger is made by National Instruments located in Austin, Texas.

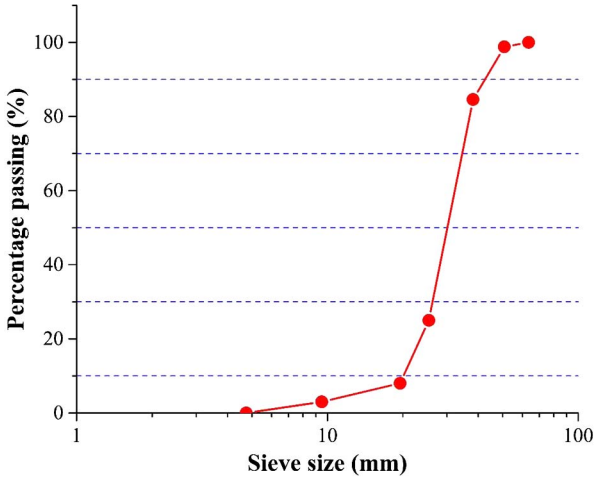

Fig. 3. Ballast gradation

Laboratory Tests

Single steel and timber crossties were used in the test. The dimensions were 2.54 × 0.16 × 0.14 m (length × width × height) for the steel crosstie and 2.59 × 0.23 × 0.18 m for the timber crosstie. Fig. 2 shows the section information of the steel crosstie. The thickness of the steel crosstie was 8 mm. The bending rigidities of the steel and the timber crossties were 0.73 and 1 MPa · m^3, respectively. The ballast gradation was classified as AREMA #4A (Fig. 3).

Calibration of Pressure Distribution Measurement System

The calibration was conducted by utilizing a materials testing system (MTS) machine. Ballast was placed in one strong wood box with the upper side open. The size of the wooden box was 0.4 × 0.4 × 0.14 m (length × width × height). One wood block cut from a timber crosstie was used as a crosstie. A pressure cell was placed between the wood block and the ballast, as shown in Fig. 4.

Pressures were calculated by dividing the recorded force from the MTS machine by the area of the pressure cell. The tie loads were transferred through the crosstie over the total area of the cell. The calculated pressures were compared to the simultaneously measured values indicated by the pressure cells, which ranged from 0 to 26,700 N.

Laboratory Testing of Pressure Distribution under Crossties

Test Setup

Five pressure cells (numbered from 24 to 28) were placed under the ties symmetrically. Figs. 5–7 show the locations of the pressure

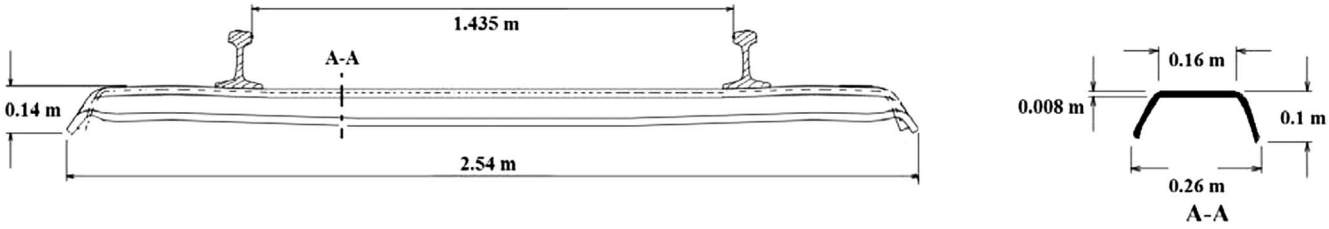

Fig. 2. Section of the steel crosstie

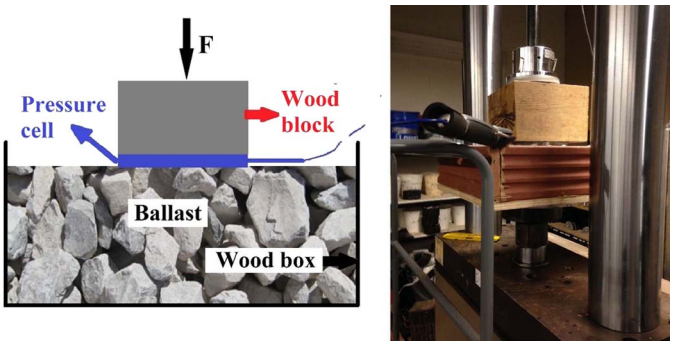

Fig. 4. Pressure calibration test (images by Weimin Song)

cells and the test setup. In Fig. 5, the distance between the two adjacent pressure cells was 0.38 m. One steel beam was placed on the rails to apply the external load at the center of the crosstie.

Research showed that the hollow steel crosstie presents a high-stress concentration under its edges (Laryea et al. 2014). To reduce the effect of stress concentration and ensure that a relatively normal pressure can be obtained, pressure cells were placed at a depth of 0.13 m beneath the crosstie rather than at the interface between ballast and crosstie, as Fig. 5 shows.

Ballast was compacted with a vibratory compactor before the placement of the pressure cell. The porosity after the ballast compaction was approximately 50%. The depth of the ballast beneath the sleeper was approximately 1 m, which meets the requirement of the AREMA specification (AREMA 2016). After the placement of the pressure cell, the ballast was leveled and the crosstie was installed above the pressure cells. Before the actual test, preloading was applied to ensure good contact between ballast and the pressure cells.

Testing Procedure

The loading and testing procedure consisted of three parts. The first part involved applying a static loading. An external force was applied from 0 to 2,20,000 N in five stages and then removed in the same manner [Fig. 8(a)]. The pressure values were measured and recorded at six load levels: 0, 44,000, 88,000, 1,32,000, 1,76,000, and 2,20,000 N. To obtain stable readings of the pressure during the loading and unloading process, a 1-min duration was used for each loading level, as shown in Fig. 8(a). Sinusoidal loading is commonly used to simulate the cyclic loading in laboratory tests (Anderson and Fair 2008; Indraratna et al. 2009; Laryea et al. 2014). After the static loading test, a cyclic loading ranging from 4,400 to 44,000 N was performed at 2 Hz for 10,000 cycles

Fig. 6. Pressure cell placement (image by Weimin Song)

[Fig. 8(b)]. Because the steel sleeper is generally used in light rail transit systems, the maximum load in the cyclic loading was selected to be 44,000 N to simulate six-axle lightweight loading. During this loading, the pressure development was recorded. After the cyclic loading, the static loading procedure was performed again in the manner previously described to evaluate the influence of the cyclic loading on the pressure distribution.

Results and Discussions

Calibration of Pressure Distribution Measurement System

The calibration was made at five loading levels: 0, 6,700, 13,400, 20,100, and 26,800 N. Three repetitive tests were performed to evaluate the repeatability of the pressure cells. Fig. 9 shows the

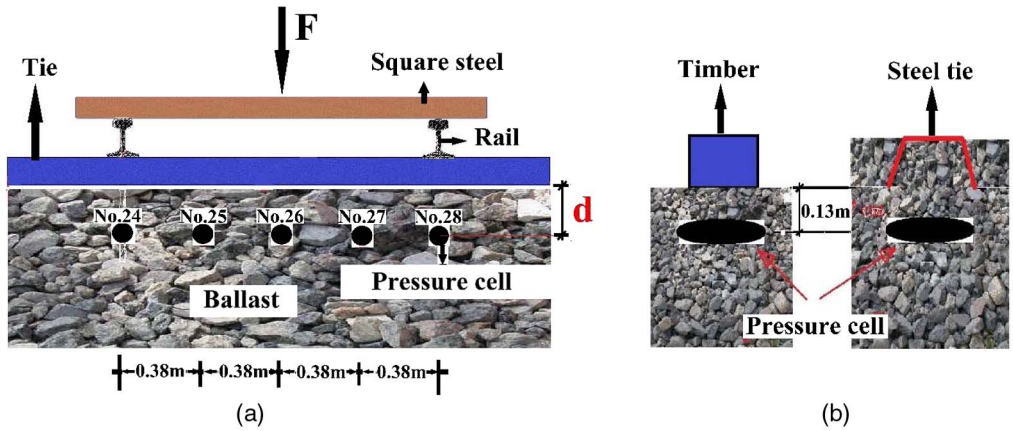

Fig. 5. Schematic diagram of the test: (a) front view; (b) lateral view (images by Weimin Song)

(a) (b)

Fig. 7. Test setup: (a) timber crosstie; (b) steel crosstie (images by Weimin Song)

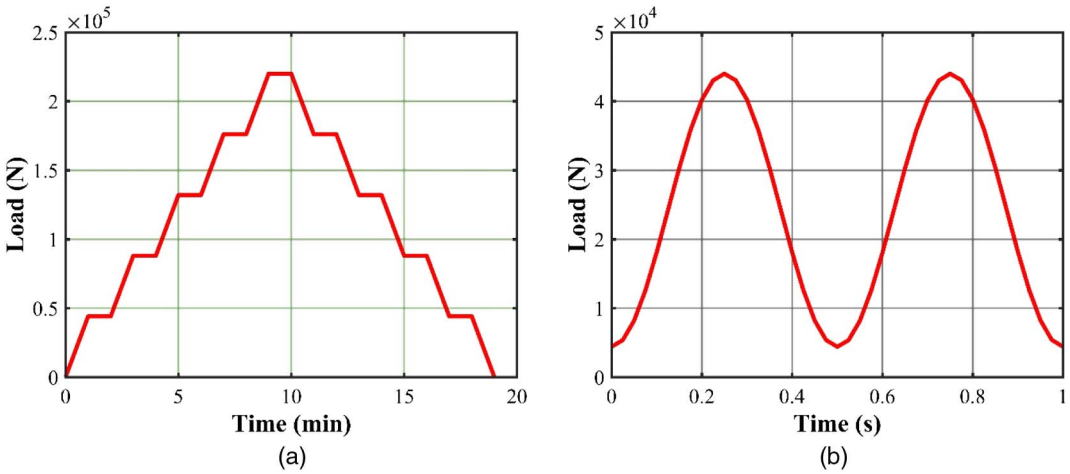

Fig. 8. (a) Static loading procedure; (b) cyclic loading procedure

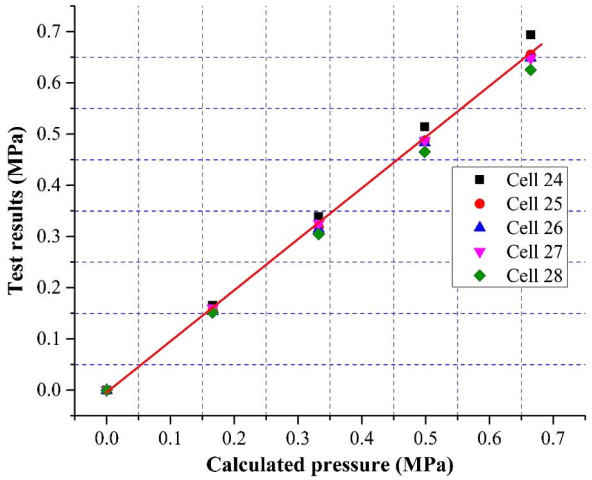

Fig. 9. Calibration of the pressure distribution system

relationship between the calculated pressures and measured pressures. There was good consistency between the calculated pressures and the measurements. The calibration results confirmed the reliability of the pressure distribution measurement system.

Results of Static and Cyclic Loading Tests

Fig. 10 displays the pressure distributions along the steel crosstie before and after the cyclic loading in the loading process from 0 to 2,20,000 N.

For the steel crosstie during the first static loading, as the external force increased, the pressure increased as well. When a low external force (44,000 and 88,000 N) was applied, the pressure at the center was higher than that at other locations. As the external force increased, the pressure at the locations halfway between the rail seat and the center (Cell 25 and Cell 26) increased markedly and became higher than the pressures at other locations. This trend continued until the highest loading level. After the 10,000-cycle dynamic loading, the pressure distribution was different from that

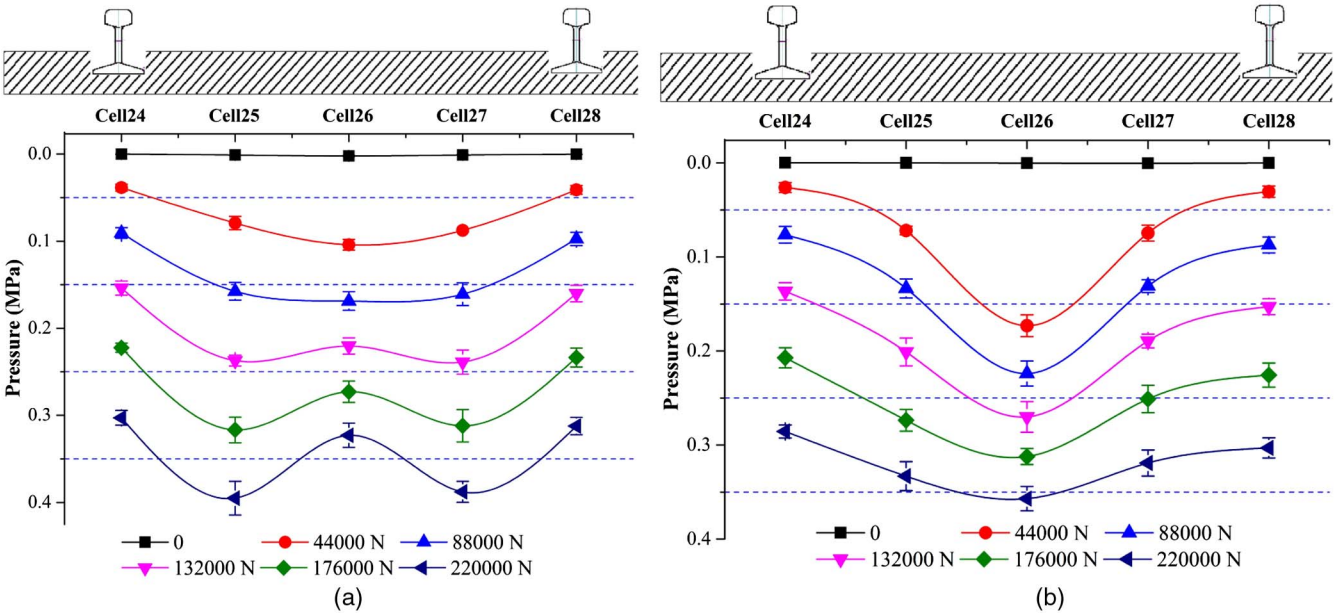

Fig. 10. Pressure distribution along the steel crosstie: (a) before cyclic loading; (b) after cyclic loading

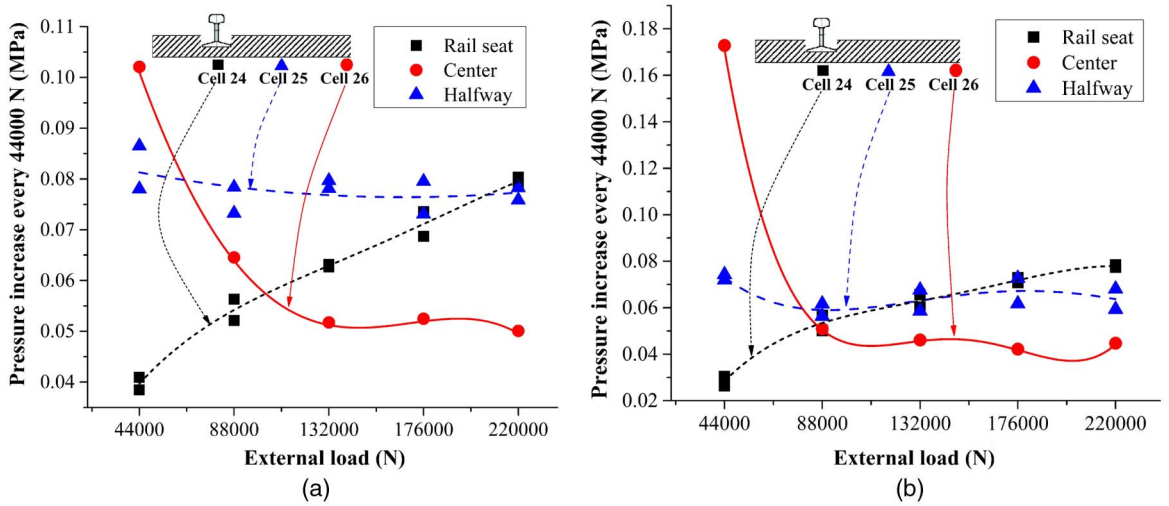

Fig. 11. Pressure increase every 44,000 N for steel crosstie: (a) before cyclic loading; (b) after cyclic loading

before the cyclic test. The pressure at the center was always the highest among all the locations at all external loading levels, and the pressures at the two ends were the lowest, which agrees with Laryea et al. (2014).

Fig. 11 presents the pressure increase at every loading level for the steel crosstie before and after cyclic loading. At the rail seat, the pressure increment at every loading level increased before and after the cyclic loading. However, the pressure increment at the halfway location between rail seat and the center remained unchanged at every loading level. For the pressure at the center, the pressure increment decreased significantly at low-level loading, and at high-loading level (1,32,000, 1,76,000, and 2,20,000 N) the pressure increment remained constant before and after the cyclic loading.

Fig. 12 shows the pressure distributions under the timber crosstie before and after the cyclic loading. As in the steel crosstie testing, the pressures under the timber crosstie all increased with the increase in the applied load. However, the increase trend was different between steel and timber crossties. At the lowest loading level (44,000 N), the pressures at the middle three locations were approximately equal, and were higher than those at both ends. As the external load increased, the pressure under the timber crosstie increased from outside to inside, indicating that the four outside locations experienced a higher increase than did the center location. This caused the two locations midway between rail seat and center to experience the highest pressure at two intermediate loading levels (88,000 and 1,32,000 N), and the two rail-seat locations experienced the highest pressure at the high loading levels (1,76.000 and 2,20,000 N). The pressure distribution under the high external loads was generally in agreement with published results (ORE 1968; Talbot 1929). As the external force increased from 44,000 to 2,20,000 N, the pressures at two rail seats increased most quickly, from 0.04 to 0.48 MPa, followed by those at the two locations midway between rail seat and center, from approximately 0.1 to about 0.42 MPa. In comparison, the center location

J. Transp. Eng., Part A: Systems, 2017, 143(9): 04017046

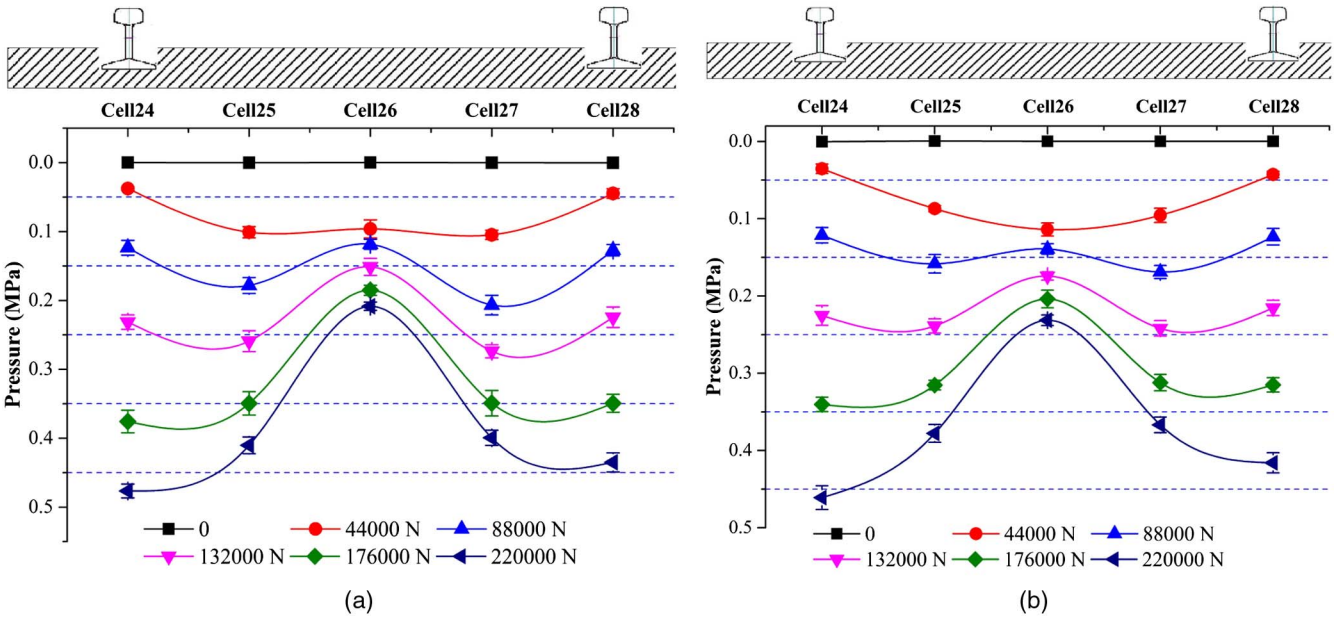

Fig. 12. Pressure distribution along the timber: (a) before cyclic loading; (b) after cyclic loading

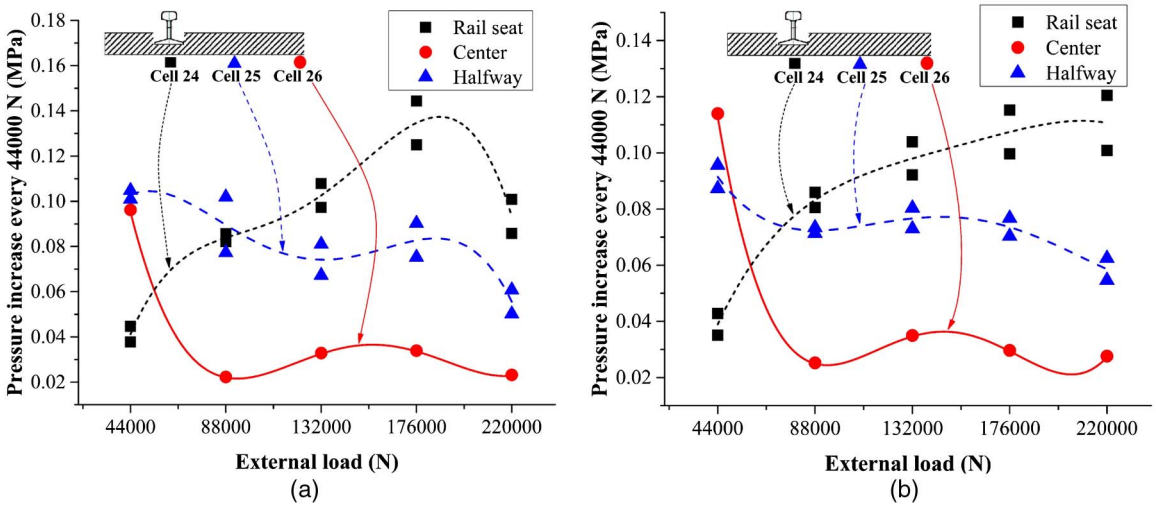

Fig. 13. Pressure increase every 44,000 N for timber crosstie: (a) before cyclic loading; (b) after cyclic loading

experienced an increase in pressure from 0.1 to only 0.21 MPa when the load was increased from 44,000 to 2,20,000 N. After the cyclic loading of 10,000 cycles, the pressure distribution was similar to that before the cyclic loading, and the only difference was that at the lowest loading level (44,000 N), the pressure at the center was highest, decreasing farther from the center.

Comparison of the pressure distribution under the steel crosstie and the timber crosstie (Figs. 10 and 12) shows that the pressure distribution under steel crosstie was more uniform than that beneath timber crosstie, especially at high loading levels. This may be because, compared with the timber sleeper, the edges of the steel crossties restricted the ballast movement in the horizontal direction and made the ballast beneath the steel crosstie more compacted.

Fig. 13 presents the pressure increment at every loading level for the timber crosstie before and after the cyclic loading. The pressure increment at the center and at the rail seat was similar to that of the steel crosstie. However, as the external load increased, the pressure increment decreased before and after the cyclic loading.

To further the understanding of the effect of the cyclic loading on the pressure distribution, the changes in maximum and minimum pressures with the loading cycles were examined. Figs. 14 and 15 show the changes in maximum and minimum pressures with the increase in loading cycles for steel and timber crossties, respectively. The maximum pressure was obtained at the external load of 44,000 N, whereas the minimum pressure value was obtained at the 4,400 N load. With the increase in loading cycles, the pressure at the center of the crosstie (Cell 26) significantly increased for both steel and timber crossties, but the pressure at the two midway locations significantly decreased. The pressure beneath the rail seats did not show much change.

Figs. 16 and 17 compare the pressures at different locations of the crosstie before and after the cyclic loading. Fig. 18 displays the percentage of the pressure change after the cyclic loading.

J. Transp. Eng., Part A: Systems, 2017, 143(9): 04017046

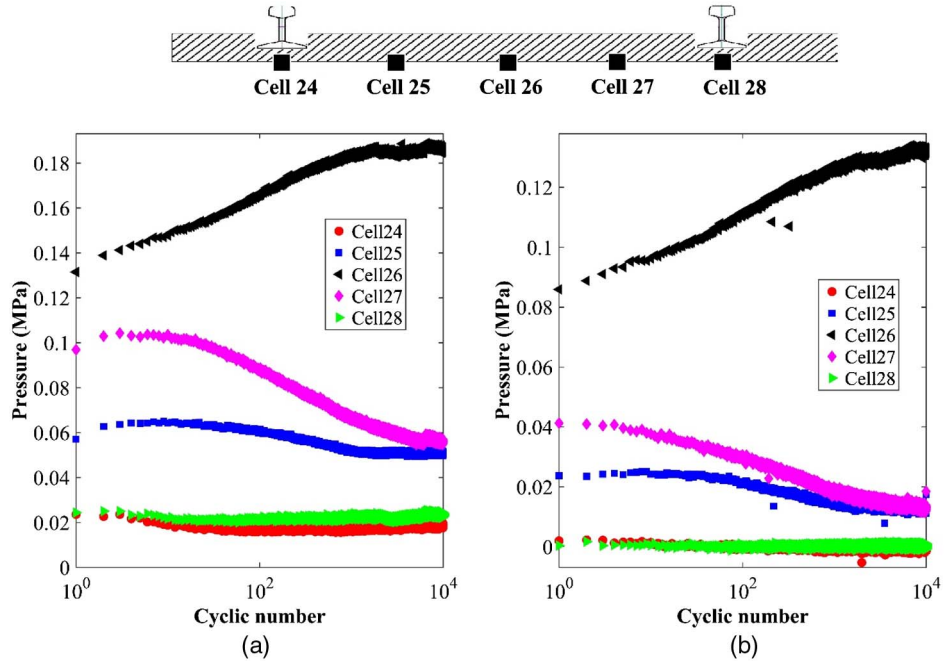

Fig. 14. Pressure development under steel crosstie during the cyclic loading: (a) maximum pressure; (b) minimum pressure

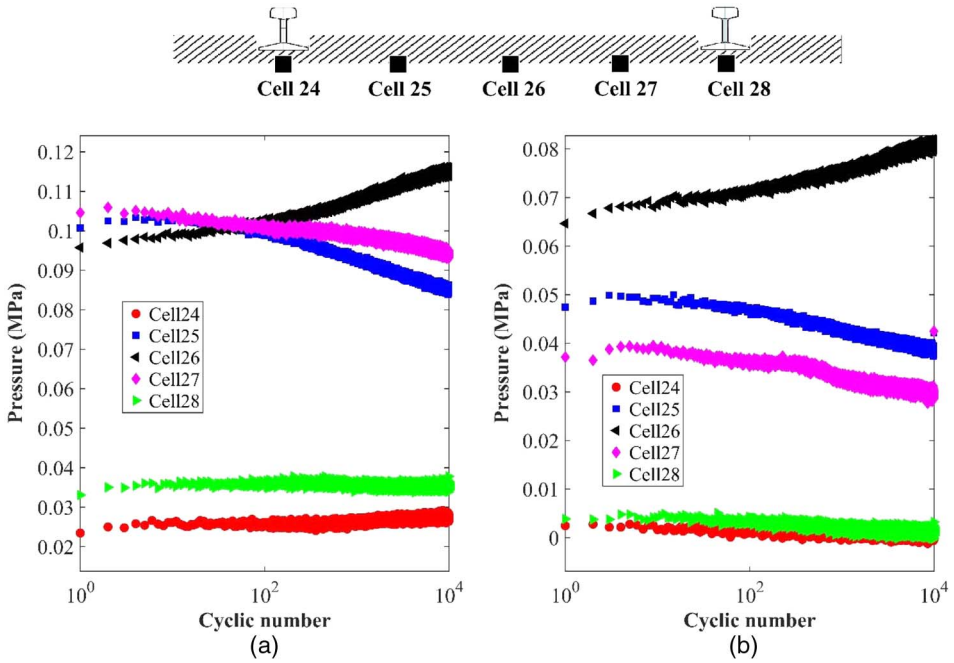

Fig. 15. Pressure development under timber crosstie during the cyclic loading: (a) maximum pressure (b) minimum pressure

For the steel crosstie, after the cyclic loading process the pressure at the rail set showed a slight decrease of approximately 6% at 2,20,000 N. The pressure at the halfway location also showed a decreasing trend with a decrease of approximately 17% at the maximum loading level. The decrease was more significant at the halfway location than at the rail seat. Unlike pressures at these two locations, the pressure at the center of the steel crosstie showed a significant increase after the cyclic loading, 13% at 2,20,000 N. This indicates that cyclic loading could improve the ballast support to the steel crosstie at the center location, but compromise the support at other locations, especially at the location halfway between the rail seat and the center. For the timber crosstie, Fig. 17 shows that as the external load increased, all the measured pressures increased, but the increase rate at the rail seat was the largest, followed those at the halfway and center locations. The pressure at the rail seat showed almost no difference before and after the cyclic loading. Similar to the steel crosstie, the pressure at the center of timber crosstie also increased after the cyclic loading, whereas the pressure decreased at the halfway location. The change in pressure was 14% for the center and −10% for the halfway location, indicating that cyclic loading could enhance ballast support n at the center of the timber and reduce the support at the halfway location.

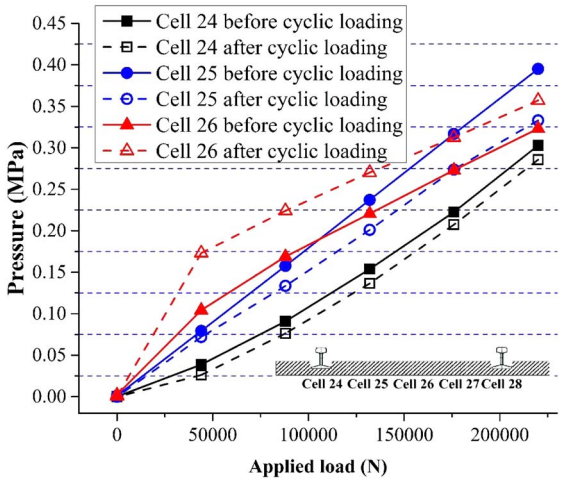

Fig. 16. Pressure comparison of steel crosstie between initial condition and after the cyclic loading

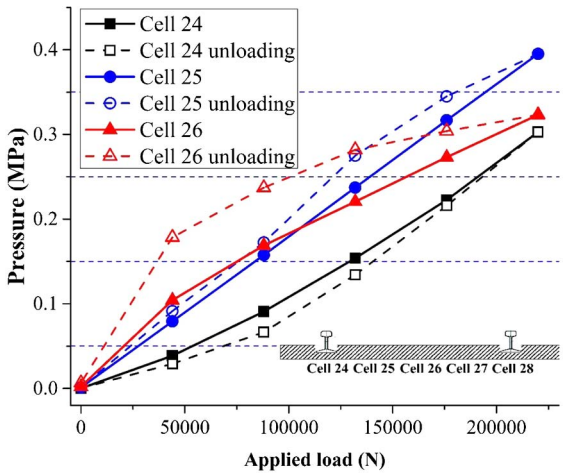

Fig. 19. Pressure comparison of steel crosstie between loading and unloading process

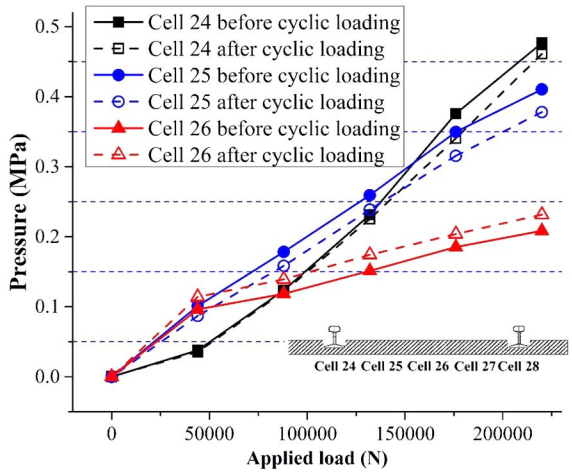

Fig. 17. Pressure comparison of timber between initial condition and after the cyclic loading

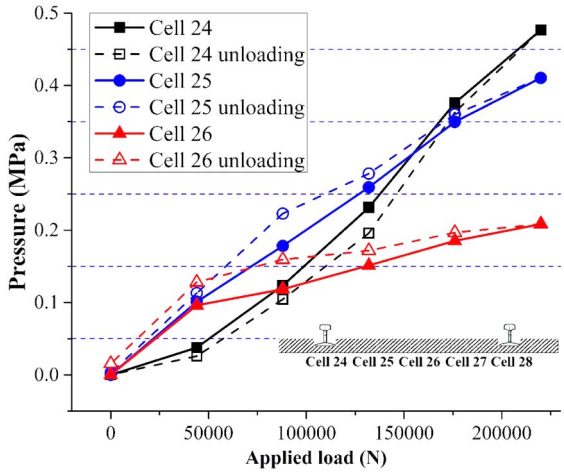

Fig. 20. Pressure comparison of timber between loading and unloading process

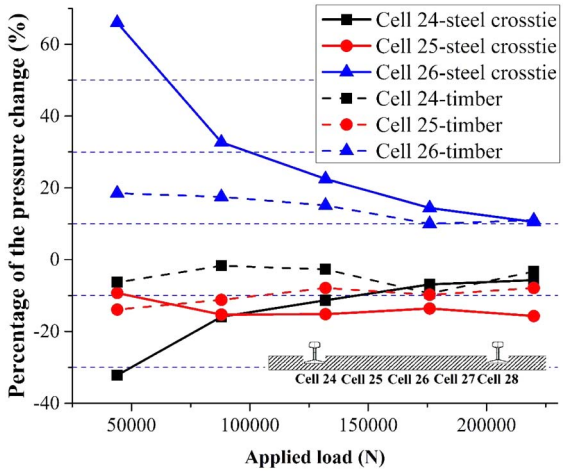

Fig. 18. Percentage of the pressure change after cyclic loading

However, comparison of the pressures under steel and timber crossties shows that the effect of the cyclic loading on the steel crosstie was more significant than on the timber for the center and halfway locations at loading levels from 44,000 to 2,20,000 N (Fig. 18). The bending rigidity values of the timber and steel crossties are 1 and 0.73 MPa · m^3, respectively. Under external loading, the steel crosstie is more easily deformed than the timber sleeper. The difference in bending rigidity between steel and timber crossties caused the pressure difference under the steel and timber crossties. Furthermore, the shapes of the steel and timber crossties are different, which may contribute to the difference in pressure under steel and timber crossties.

The pressures of the five cells also were recorded during the unloading process from 2,20,000 to 0 N. Figs. 19 and 20 compare pressures obtained from the loading and unloading processes. The pressure results were obtained during the first static loading test prior to the cyclic loading. For both the steel and timber crossties, the pressures obtained during the unloading process at the rail seat were lower than the corresponding values obtained from the

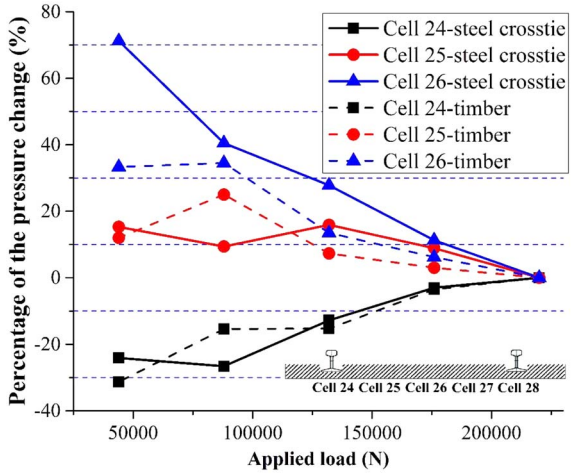

Fig. 21. Percentage of the pressure change after the unloading process

loading process, but the opposite was observed for pressures at the halfway and center locations. Fig. 21 shows the percentage of the pressure change after the unloading process. At the halfway and center locations, the general trend was that the percentage increase in pressure under the steel crosstie was larger than that under the timber crosstie. The percentage decrease of the pressure beneath the rail seat was similar for the steel and the timber crossties at the different loading levels in this study.

Conclusions

A laboratory study investigated the pressure distribution characteristics under a single steel or timber crosstie. Five pressure cells were equidistantly located under the crossties between the two rail seats. The pressure measurement system first was calibrated, then static and cyclic loadings were applied in the laboratory test. The difference in pressure distribution was analyzed between the steel and timber crossties. The effect of cyclic loading on the pressure distribution under the crossties also was examined. The following conclusions can be drawn from this study:

- The pressure measurement system was reliable for measuring the pressure distribution under the steel and timber crossties.
- In the static loading test, at a low loading level (44,000 and 88,000 N) the pressure at the center of the steel crosstie was the highest among all the pressures measured at different locations. As the applied load increased, the pressures at the location halfway between the rail seat and the center gradually became the highest. However, for the timber crosstie, with the increase in the loading level the maximum pressure was obtained directly beneath the rail seats.
- Cyclic loading could increase the pressure at the center of the crosstie and significantly decrease the pressure at the locations halfway between the rail seat and the center. The pressures beneath the rail seats showed a slight decrease.
- The effect of the cyclic loading on the pressure distribution of the steel crosstie was more significant than that on the pressure distribution of the timber crosstie.
- A difference in pressure distribution existed between the loading and unloading processes. For both the steel and timber crossties, the pressures obtained from the unloading process beneath the rail seats were lower than those from the unloading process, but the pressures at other locations were higher from the unloading process than from the loading process at the same loading level.

Acknowledgments

The authors would like to thank the financial sponsorship provided by the U.S. DOT through the National University Rail Center (NURail). The authors would also like to thank Dr. Xiaoyang Jia, Mr. Yongjie Ding, Mr. Wei Hu, Mr. Bingye Han, and Mr. Pawel Andrzej for their assistance in this project. The contents of this study reflect the views of the authors only. The first author would also appreciate the financial support provided by the China Scholarship Council (CSC).

References

Anderson, J. S., and Rose, J. G. (2008). "In-situ test measurement techniques within railway track structures." *Proc., IEEE/ASME/ASCE 2008 Joint Rail Conf.*, ASME, New York, 187–207.

Anderson, W. F., and Fair, P. (2008). "Behavior of railroad ballast under monotonic and cyclic loading." *J. Geotech. Geoenviron. Eng.*, 10.1061/(ASCE)1090-0241(2008)134:3(316), 316–327.

AREMA (American Railway Engineering and Maintenance-of-Way Association). (2016). *Manual for railway engineering*, Simmons-Boardman Publishing, Halethorpe, MD.

Brinckerhoff, P. (2012). *Track design handbook for light rail transit*, National Academy of Sciences, Washington, DC, 4–7.

Csenge, M. V., Wolf, H. E., Dersch, M. S., Edwards, J. R., Kernes, R. G., and Romero, M. G. (2015). "Exploration of alternatives for prestressed concrete monoblock crosstie design based on flexural capacity." *Proc., 2015 Joint Rail Conf.*, ASME, New York.

Hossain, Z., Indraratna, B., Darve, F., and Thakur, P. (2007). "DEM analysis of angular ballast breakage under cyclic loading." *Geomech. Geoeng.: Int. J.*, 2(3), 175–181.

Indraratna, B., Thakur, P. K., and Vinod, J. S. (2009). "Experimental and numerical study of railway ballast behavior under cyclic loading." *Int. J. Geomech.*, 10.1061/(ASCE)GM.1943-5622.0000055, 136–144.

Jia, G., Zhan, T. L., Chen, Y., and Fredlund, D. (2009). "Performance of a large-scale slope model subjected to rising and lowering water levels." *Eng. Geol.*, 106(1), 92–103.

Kuo, C.-M., and Huang, C.-H. (2009). "Two approaches of finite-element modeling of ballasted railway track." *J. Geotech. Geoenviron. Eng.*, 10.1061/(ASCE)1090-0241(2009)135:3(455), 455–458.

Laryea, S., Baghsorkhi, M. S., Ferellec, J., McDowell, G., and Chen, C. (2014). "Comparison of performance of concrete and steel sleepers using experimental and discrete element methods." *Transp. Geotech.*, 1(4), 225–240.

McHenry, M. T., Brown, M., LoPresti, J., Rose, J., and Souleyrette, R. (2015). "Use of matrix-based tactile surface sensors to assess fine-scale ballast-tie interface pressure distribution in railroad track." *J. Transp. Res. Board*, 2476, 23–31.

ORE (Office of Research and Experiments). (1968). "Stress in the rails." *Rep. No. D71/RP9/E*, Office of Research and Experiments of the International Union of Railways, Utrecht, Netherlands.

Rapp, C., Dersch, M., Edwards, J., Barkan, C., Wilson, B., and Mediavilla, J. (2013). "Measuring rail seat pressure distribution in concrete crossties: Experiments with matrix-based tactile surface sensors." *J. Transp. Res. Board*, 2374, 190–200.

Recuero, A., Escalona, J., and Shabana, A. (2011). "Finite-element analysis of unsupported sleepers using three-dimensional wheel–rail contact formulation." *Proc. Inst. Mech. Eng. Part K: J. Multi-body Dyn.*, 225(2), 153–165.

Rose, J., Su, B., and Twehues, F. (2004). "Comparisons of railroad track and substructure computer model predictive stress values and in-situ stress measurements." *Proc., AREMA 2004 Annual Conf. and Exposition*, AREMA, Lanham, MD.

Sadeghi, J. (2008). "Experimental evaluation of accuracy of current practices in analysis and design of railway track sleepers." *Can. J. Civ. Eng.*, 35(9), 881–893.

Sadeghi, J. (2010). "Field investigation on dynamics of railway track pre-stressed concrete sleepers." *Adv. Struct. Eng.*, 13(1), 139–151.

Sun, Q. D., Indraratna, B., and Nimbalkar, S. (2015). "Deformation and degradation mechanisms of railway ballast under high frequency cyclic loading." *J. Geotech. Geoenviron. Eng.*, 10.1061/(ASCE)GT.1943-5606.0001375, 04015056.

Talbot, A. (1929). "Fifth progressive report of especial committee on stresses in rail road track." *Proc. AREA*, 30, 34–35.

Wolf, H. E., Edwards, J. R., Dersch, M. S., and Barkan, C. P. (2015). "Flexural analysis of prestressed concrete monoblock sleepers for heavy-haul applications: Methodologies and sensitivity to support conditions." *Proc., 11th Int. Heavy Haul Association Conf.*, Univ. of Illinois at Urbana-Champaign, Champaign, IL.